2024 European Control Conference (ECC)
June 25-28, 2024. Stockholm, Sweden

Implementation aspects for state and parameter observers for induction machines at low sample-to-fundamental frequency ratios

Georg Janisch[1], Andreas Kugi[1,2] and Wolfgang Kemmetmüller[1]

***Abstract*— The current developments in electric drive systems are directed towards high rotational speeds and partial operation in the (thermal) overload range. This makes nonlinear control theory increasingly common as the demands of high-performance drives increase, and high computing power becomes more accessible and available. However, high-speed drives are also confronted with a low sample-to-fundamental frequency ratio, which is particularly challenging for the observer design. In this case, the accurate timing of the measurements within the pulse-width modulation (PWM) pattern becomes relevant but is mostly neglected in the observer design. Therefore, this work investigates essential aspects of developing nonlinear state and parameter observers (extended Kalman filter) for induction machines, especially considering the timing of the PWM and current measurements. An observer is proposed, which systematically takes into account these effects. Simulation and measurement results prove that the proposed observer significantly improves estimation accuracy compared to the state of the art when electric drives with a low sample-to-fundamental frequency are considered.**

I. Introduction

Typical requirements for electric drives are to be efficient and powerful while having low costs and compact size. These requirements are in partial conflict and, thus, need to be weighted according to the application [1]. Observers can help to increase efficiency and accuracy. Furthermore, the costs of the drive can be reduced by replacing complex sensors that would be required to measure all system states. Observers can also be extended to estimate parameters necessary to achieve high control accuracy in cases where the parameters change during operation. In the example of an induction machine, a state observer is required for closed-loop operation to avoid costly flux-measuring coils or current measurement at the rotor. Furthermore, the rotor time constant changes due to the temperature variations and thus must be estimated if a costly temperature sensor should be avoided [2].

This work considers the challenges arising from the observer design for induction motors used as the traction drive in electromobility. In this application, costs must be kept low for high production volumes; therefore, only a minimum number of sensors is available. One specific challenge is that the high speed, in combination with the limited PWM frequency that typically occurs in these applications, results in a low sample-to-fundamental frequency ratio [3], [4], [5].

Classic observers for induction machines are based either on a voltage model of the stator or on a current model of the stator, see, e.g., [6]. An intuitive combination of both models is the Gopinath-style observer [7]. This observer topology uses the transfer function of the voltage model with a feedback loop of the current model. The dynamic behavior of the resulting observer is related to the choice of the poles of the feedback loop. This observer is extensively studied in the literature, primarily for direct torque and flux control applications [8], [9], [10]. Time discretization of the observer is required for the implementation on real-time hardware. If the sampling frequency of the observer is sufficiently high compared to the drive's electric fundamental frequency, the exact form of the time discretization is not critical. Since this assumption is frequently valid, the basic Gopinath-style observer yields good results. However, there is a clear trend to very high rotational speed applications in recent years, which results in increasing demands for the time synchronization of the voltage and the current model and the specific form of time-discretization. E.g., [11] and [5] extended the Gopinath-style observer type for low sample-to-fundamental frequency ratios. In particular, [11] extends the observer design by a further current observer, and [5] exchanges the voltage model equations by a model not using stator current information. However, these extensions of the basic Gopinath-style observer complicate the overall dynamic behavior, and thus, the tuning of the observer. This problem becomes even more severe when parameter observers extend the state observer since then, a coupled system of multiple observers must be considered [12].

Another approach of state and parameter estimators for induction machines is the design of observers in the state space instead of frequency space. These observers (referred to as Kubota-style observers in the literature [13]) include Luenberger observers and (nonlinear) Kalman filters [2]. Extended Kalman Filters (EKFs) provide a systematic design, which allows the inclusion of models with magnetic nonlinearities [14] and the design of state and parameter observers in a single step. However, time discretization is also important in drives with low sample-to-fundamental frequency ratios. A modified Euler method is proposed in [15] to tackle this problem. However, no specific investigations on the update step inherent to a (nonlinear) Kalman filter have been reported for low sample-to-fundamental frequency applications.

Therefore, this work focuses on the implementation aspects of a Kubota-style observer (EKF) for an induction machine, which are relevant for low sample-to-fundamental frequencies. The task is to estimate the state variables, the rotor resistance, and the mutual inductance within one

[1]Automation and Control Institute, TU Wien, Vienna, Austria {janisch, kugi, kemmetmueller}@acin.tuwien.ac.at
[2]Austrian Institute of Technology, Vienna, Austria

observer. The work [16] used a time-continuous Kalman filter for this configuration, and [17] investigated it in simulations. It is an advantageous combination of state and parameter estimation since estimating the rotor time constant would be sensitive to errors in the mutual inductance [18], which varies with the flux linkage level due to saturation [19].

The main contribution of this paper is a systematic and meticulous study of the synchronization between current measurements and the pulse-width modulation (PWM) pattern. In particular, the position of the current measurements at the center of a PWM period is crucial for the correction step of the observer. Another indispensable factor in achieving high observer accuracy is the choice of the time-discretization method for the prediction step. It will be shown by simulation and measurement results that these practical aspects are of significant importance in attaining the required estimation accuracy when confronted with scenarios characterized by low sample-to-fundamental frequency ratios.

The paper is structured as follows: In Section II, the induction machine model is introduced, including modeling the current measurement, and a discrete-time formulation. Section III presents the observer design, and simulation and experimental results are given in Section IV.

II. Model

A. Induction machine model

A Γ space vector model of an induction machine is used within this work. Therein, all quantities $\mathbf{x}$ of the model are represented in the orthogonal $\alpha\beta-$frame, i.e., $\mathbf{x}_{\alpha\beta} = [x_\alpha, x_\beta]^{\mathrm{T}}$, that are related to the three-phase quantities $\mathbf{x}_{\mathrm{abc}} = [x_{\mathrm{a}}, x_{\mathrm{b}}, x_{\mathrm{c}}]^{\mathrm{T}}$ via the power invariant Clarke transformation [20],

$$\mathbf{x}_{\alpha\beta} = \mathbf{T}\mathbf{x}_{\mathrm{abc}}, \qquad \mathbf{T} = \sqrt{\frac{2}{3}}\begin{bmatrix} 1 & -\frac{1}{2} & -\frac{1}{2} \\ 0 & \frac{\sqrt{3}}{2} & -\frac{\sqrt{3}}{2} \end{bmatrix}. \tag{1}$$

The Γ-model of a squirrel cage induction machine in a stator-fixed reference frame reads as

$$\frac{\mathrm{d}\boldsymbol{\Psi}_{\mathrm{s}}}{\mathrm{d}t} = -R_{\mathrm{s}}\mathbf{i}_{\mathrm{s}} + \mathbf{u}_{\mathrm{s}} \tag{2a}$$

$$\frac{\mathrm{d}\boldsymbol{\Psi}_{\mathrm{r}}}{\mathrm{d}t} = -R_{\mathrm{r}}\mathbf{i}_{\mathrm{r}} + \omega\mathbf{J}\boldsymbol{\Psi}_{\mathrm{r}}, \tag{2b}$$

with the stator flux $\boldsymbol{\Psi}_{\mathrm{s}}$, the rotor flux $\boldsymbol{\Psi}_{\mathrm{r}}$, the stator voltage $\mathbf{u}_{\mathrm{s}}$, the stator current $\mathbf{i}_{\mathrm{s}}$, the rotor current $\mathbf{i}_{\mathrm{r}}$, the stator resistance R_{s}, and the rotor resistance R_{r}, see, e.g., [20]. $\omega = \omega_{\mathrm{m}} Z_{\mathrm{p}}$ is the electrical speed, with the mechanical angular speed ω_{m} and the number of pole pairs Z_{p}. The orthogonal rotation matrix $\mathbf{J}$ is defined as

$$\mathbf{J} = \begin{bmatrix} 0 & -1 \\ 1 & 0 \end{bmatrix}. \tag{3}$$

The rotor and stator flux are described by the flux linkage equations in the form

$$\boldsymbol{\Psi}_{\mathrm{s}} = M\left(\mathbf{i}_{\mathrm{s}} + \mathbf{i}_{\mathrm{r}}\right) \tag{4a}$$

$$\boldsymbol{\Psi}_{\mathrm{r}} = L_\sigma \mathbf{i}_{\mathrm{r}} + \boldsymbol{\Psi}_{\mathrm{s}}, \tag{4b}$$

with the mutual inductance M and the leakage inductance L_σ. Applying the co-energy principle gives the torque T of the machine in the form

$$T = \frac{Z_{\mathrm{p}}}{L_\sigma}\boldsymbol{\Psi}_{\mathrm{s}}^{\mathrm{T}}\mathbf{J}\boldsymbol{\Psi}_{\mathrm{r}}. \tag{5}$$

Using the state $\mathbf{x}^{\mathrm{T}} = \left[\boldsymbol{\Psi}_{\mathrm{s}}^{\mathrm{T}},\ \boldsymbol{\Psi}_{\mathrm{r}}^{\mathrm{T}}\right]^{\mathrm{T}}$ and eliminating the stator current

$$\mathbf{i}_{\mathrm{s}} = \begin{bmatrix} \frac{M+L_\sigma}{L_\sigma M} & 0 & -\frac{1}{L_\sigma} & 0 \\ 0 & \frac{M+L_\sigma}{L_\sigma M} & 0 & -\frac{1}{L_\sigma} \end{bmatrix}\begin{bmatrix} \boldsymbol{\Psi}_{\mathrm{s}} \\ \boldsymbol{\Psi}_{\mathrm{r}} \end{bmatrix} \tag{6}$$

and rotor current $\mathbf{i}_{\mathrm{r}} = (\boldsymbol{\Psi}_{\mathrm{r}} - \boldsymbol{\Psi}_{\mathrm{s}})/L_\sigma$ results in the state-space representation

$$\frac{\mathrm{d}}{\mathrm{d}t}\begin{bmatrix} \boldsymbol{\Psi}_{\mathrm{s}} \\ \boldsymbol{\Psi}_{\mathrm{r}} \end{bmatrix} = \mathbf{A}\begin{bmatrix} \boldsymbol{\Psi}_{\mathrm{s}} \\ \boldsymbol{\Psi}_{\mathrm{r}} \end{bmatrix} + \begin{bmatrix} 1 & 0 \\ 0 & 1 \\ 0 & 0 \\ 0 & 0 \end{bmatrix}\mathbf{u}_{\mathrm{s}} = \mathbf{A}\mathbf{x} + \mathbf{B}\mathbf{u}_{\mathrm{s}}, \tag{7}$$

with

$$\mathbf{A} = \begin{bmatrix} -R_{\mathrm{s}}\frac{L_\sigma+M}{L_\sigma M} & 0 & \frac{R_{\mathrm{s}}}{L_\sigma} & 0 \\ 0 & -R_{\mathrm{s}}\frac{L_\sigma+M}{L_\sigma M} & 0 & \frac{R_{\mathrm{s}}}{L_\sigma} \\ \frac{R_{\mathrm{r}}}{L_\sigma} & 0 & -\frac{R_{\mathrm{r}}}{L_\sigma} & -\omega \\ 0 & \frac{R_{\mathrm{r}}}{L_\sigma} & \omega & -\frac{R_{\mathrm{r}}}{L_\sigma} \end{bmatrix}. \tag{8}$$

B. Voltage signal

A two-level PWM inverter with the dc link voltage u_{dc} and the PWM frequency f_{s} drives the machine. A center symmetric PWM waveform is used, which yields the three terminal voltages

$$u_n = \begin{cases} 0 & kT_{\mathrm{s}} \le t < T_{\mathrm{s}}\left(k + \frac{1-\chi_{n,k}}{2}\right) \\ u_{\mathrm{dc}} & T_{\mathrm{s}}\left(k + \frac{1-\chi_{n,k}}{2}\right) \le t < T_{\mathrm{s}}\left(k + \frac{1+\chi_{n,k}}{2}\right) \\ 0 & T_{\mathrm{s}}\left(k + \frac{1+\chi_{n,k}}{2}\right) \le t < (k+1)\,T_{\mathrm{s}} \end{cases} \tag{9}$$

for $n \in \{a, b, c\}$. Therein, it is assumed that during one PWM cycle of length $T_{\mathrm{s}} = 1/f_{\mathrm{s}}$ (sampling time), the duty cycle $\boldsymbol{\chi}_{\mathrm{abc},k} = [\chi_{\mathrm{a},k},\ \chi_{\mathrm{b},k},\ \chi_{\mathrm{c},k}]^{\mathrm{T}}$, $0 \le \chi_{n,k} \le 1$, of the three phases is kept constant. The time index k is used to denote the value of a discrete-time or continuous-time signal at $t = kT_{\mathrm{s}}$.

For the subsequent observer design, a simplified model utilizing the average voltages over one PWM cycle $\bar{\mathbf{u}}_{abc,k} = u_{\mathrm{dc}}\boldsymbol{\chi}_{\mathrm{abc},k}$ and $\bar{\mathbf{u}}_{\mathrm{s},k} = u_{\mathrm{dc}}\boldsymbol{\chi}_{\alpha\beta,k}$ will be used. This simplification significantly reduces the complexity and corresponds to the state of the art for PWM signals [21].

C. Current measurement

Two ways of measuring the stator current are investigated. In the first method, the stator currents of the machine are measured by oversampling and averaging over one PWM cycle in the form

$$\breve{\mathbf{i}}_{\mathrm{abc},k} = \frac{1}{N}\sum_{j=0}^{N-1}\mathbf{i}_{\mathrm{abc}}\left(\left(k - 1 + \frac{j}{N}\right)T_{\mathrm{s}}\right) \tag{10}$$

with the oversampling ratio N. Consequently, $\breve{\mathbf{i}}_{\mathrm{s},k} = \mathbf{T}\breve{\mathbf{i}}_{\mathrm{abc},k}$ holds. The second, simpler method utilizes a single current measurement in the center of the PWM period, i.e.

$$\tilde{\mathbf{i}}_{\mathrm{abc},k} = \mathbf{i}_{\mathrm{abc}}\left(\left(k-\frac{1}{2}\right)T_\mathrm{s}\right) \tag{11}$$

and thus $\tilde{\mathbf{i}}_{\mathrm{s},k} = \mathbf{T}\tilde{\mathbf{i}}_{\mathrm{abc},k}$.

D. Design model

Based on these sub-models, the overall design model for the observer can be derived. The model is extended by the uncertain model parameters R_r and M, which are assumed to be unknown but constant, cf. [22]. This yields the extended state $\mathbf{x}_\mathrm{obs} = [\Psi_{\mathrm{s},\alpha}, \Psi_{\mathrm{s},\beta}, \Psi_{\mathrm{r},\alpha}, \Psi_{\mathrm{r},\beta}, M, R_\mathrm{r}]^\mathrm{T}$ and renders the model nonlinear. Additionally, process noise $\mathbf{w} = [w_{\mathrm{s},\alpha}, w_{\mathrm{s},\beta}, w_{\mathrm{r},\alpha}, w_{\mathrm{r},\beta}, w_M,\ w_{R_\mathrm{r}}]^\mathrm{T}$ and measurement noise $\mathbf{v} = \left[v_{i_{\mathrm{s}\alpha}}\ v_{i_{\mathrm{s}\beta}}\right]^\mathrm{T}$ considered for the observer design. The system equations for the observer design then read as

$$\underbrace{\frac{\mathrm{d}}{\mathrm{d}t}\begin{bmatrix}\Psi_{\mathrm{s},\alpha}\\ \Psi_{\mathrm{s},\beta}\\ \Psi_{\mathrm{r},\alpha}\\ \Psi_{\mathrm{r},\beta}\\ M\\ R_\mathrm{r}\end{bmatrix}}_{\mathbf{x}_\mathrm{obs}} = \underbrace{\begin{bmatrix}\mathbf{A}\,(M,R_\mathrm{r})\\ \mathbf{0}\end{bmatrix}\begin{bmatrix}\Psi_{\mathrm{s},\alpha}\\ \Psi_{\mathrm{s},\beta}\\ \Psi_{\mathrm{r},\alpha}\\ \Psi_{\mathrm{r},\beta}\\ M\\ R_\mathrm{r}\end{bmatrix} + \begin{bmatrix}\bar{\mathbf{u}}_\mathrm{s}\\ \mathbf{0}\end{bmatrix} + \begin{bmatrix}w_{\mathrm{s},\alpha}\\ w_{\mathrm{s},\beta}\\ w_{\mathrm{r},\alpha}\\ w_{\mathrm{r},\beta}\\ w_M\\ w_{R_\mathrm{r}}\end{bmatrix}}_{\mathbf{f}(\mathbf{x}_\mathrm{obs},\mathbf{u},\mathbf{w})} \tag{12}$$

and the stator current (6) is used as the measured system output

$$\mathbf{y} = \begin{bmatrix}i_{\mathrm{s},\alpha}\\ i_{\mathrm{s},\beta}\end{bmatrix} + \begin{bmatrix}v_{i_{\mathrm{s}\alpha}}\\ v_{i_{\mathrm{s}\beta}}\end{bmatrix} = \mathbf{h}\left(\mathbf{x}_\mathrm{obs}\right) + \mathbf{v}_k. \tag{13}$$

The nonlinear differential equation (12) must be solved in the predictor step of the nonlinear observer (extended Kalman filter, EKF). The explicit Euler method is frequently used for this task due to its simplicity [14]. However, at low sample-to-fundamental frequency ratios, the method can lead to inaccurate solutions and even result in an unstable system, e.g., [23], [15]. Therefore, the more accurate explicit fourth-order Runge-Kutta method is used for the discrete-time representation of the system. For a time step $T_\mathrm{s}/2$, this method is given in the form

$$\mathbf{x}_{\mathrm{obs},k+\frac{1}{2}} = \underbrace{\mathbf{x}_{\mathrm{obs},k} + \frac{T_\mathrm{s}}{2}\mathbf{f}_\mathrm{s}\left(\mathbf{x}_{\mathrm{obs},k}, \bar{\mathbf{u}}_{\mathrm{s},k}, \mathbf{w}_k\right)}_{\mathbf{F}(\mathbf{x}_{\mathrm{obs},k},\bar{\mathbf{u}}_{\mathrm{s},k},\mathbf{w}_k)} \tag{14a}$$

$$\mathbf{y}_k = \mathbf{h}\left(\mathbf{x}_{\mathrm{obs},k}\right) + \mathbf{v}_k = \mathbf{i}_{\mathrm{s},k} + \mathbf{v}_k, \tag{14b}$$

with

$$\mathbf{k}_1 = \mathbf{f}\left(\mathbf{x}_{\mathrm{obs},k}, \bar{\mathbf{u}}_{\mathrm{s},k}, \mathbf{w}_k\right) \tag{15a}$$

$$\mathbf{k}_2 = \mathbf{f}\left(\mathbf{x}_{\mathrm{obs},k} + \frac{T_\mathrm{s}}{4}\mathbf{k}_1, \bar{\mathbf{u}}_{\mathrm{s},k}, \mathbf{w}_k\right) \tag{15b}$$

$$\mathbf{k}_3 = \mathbf{f}\left(\mathbf{x}_{\mathrm{obs},k} + \frac{T_\mathrm{s}}{4}\mathbf{k}_2, \bar{\mathbf{u}}_{\mathrm{s},k}, \mathbf{w}_k\right) \tag{15c}$$

$$\mathbf{k}_4 = \mathbf{f}\left(\mathbf{x}_{\mathrm{obs},k} + \frac{T_\mathrm{s}}{2}\mathbf{k}_3, \bar{\mathbf{u}}_{\mathrm{s},k}, \mathbf{w}_k\right) \tag{15d}$$

$$\mathbf{f}_\mathrm{s} = \frac{1}{6}\left(\mathbf{k}_1 + 2\mathbf{k}_2 + 2\mathbf{k}_3 + \mathbf{k}_4\right). \tag{15e}$$

III. Observer design

As mentioned before, adding the parameters to the state to be estimated yields a nonlinear system. Thus, applying nonlinear observers to achieve high estimation accuracy is meaningful. In this work, an EKF is designed using the machine model from Section II. Toylat et al. reviewed different state and parameter estimation methods in [2]. It is mentioned that the disadvantage of an EKF is that it is computationally expensive. However, the substantial increase in computing power in recent years has rendered EKF feasible even for high-speed applications. The basic approach of the observer is similar to [16] and [17], where the machine parameters M and R_r are also estimated in addition to the flux linkages. However, in these works, the relevant timing aspects for low sample-to-fundamental frequency ratios are not systematically considered.

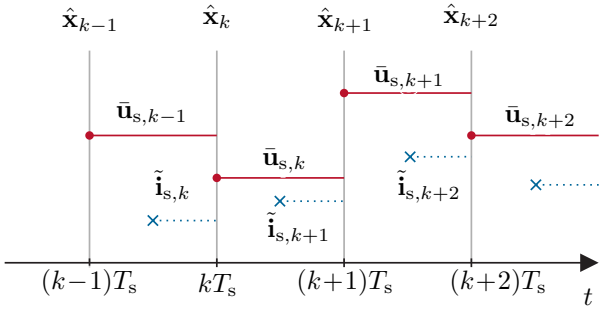

Fig. 1. Timing diagram for the observer design.

As explained in [24], the measured current values correspond to the values in the middle of the PWM period, regardless of whether the sensor system measures the current in the center of the period (11) or by oversampling (10), see Figure 1. This effect is taken into account by discretizing the system by half-period steps. The current measurement system $\tilde{\mathbf{i}}_{\mathrm{s},k}$, which is defined at $t = \left(k-\frac{1}{2}\right)T_\mathrm{s}$, is used for the corrector step with the output equation (14b), i.e. $\mathbf{y}_{k-\frac{1}{2}} = \tilde{\mathbf{i}}_{\mathrm{s},k}$. The corrector step of the proposed EKF then reads as

$$\mathbf{C} = \left.\frac{\partial}{\partial \mathbf{x}_\mathrm{obs}}\mathbf{h}\left(\mathbf{x}_\mathrm{obs}\right)\right|_{\mathbf{x}_\mathrm{obs}=\hat{\mathbf{x}}^-_{\mathrm{obs},k-\frac{1}{2}}} \tag{16a}$$

$$\mathbf{L} = \mathbf{P}^-_{k-\frac{1}{2}}\mathbf{C}^\mathrm{T}\left(\mathbf{C}\mathbf{P}^-_{k-\frac{1}{2}}\mathbf{C}^\mathrm{T} + \mathbf{R}\right)^{-1} \tag{16b}$$

$$\hat{\mathbf{y}}^-_{k-\frac{1}{2}} = \mathbf{h}\left(\hat{\mathbf{x}}^-_{\mathrm{obs},k-\frac{1}{2}}\right) \tag{16c}$$

$$\hat{\mathbf{x}}^+_{\mathrm{obs},k-\frac{1}{2}} = \hat{\mathbf{x}}^-_{\mathrm{obs},k-\frac{1}{2}} + \mathbf{L}\left(\mathbf{y}_{k-\frac{1}{2}} - \hat{\mathbf{y}}^-_{k-\frac{1}{2}}\right) \tag{16d}$$

$$\mathbf{P}^+_{k-\frac{1}{2}} = \left(\mathbf{I} - \mathbf{L}\mathbf{C}\right)\mathbf{P}^-_{k-\frac{1}{2}}, \tag{16e}$$

with the identity matrix $\mathbf{I}$. The predictor step from $\hat{\mathbf{x}}^+_{\mathrm{obs},k-\frac{1}{2}}$

to $\hat{\mathbf{x}}^+_{\mathrm{obs},k}$ is given by using $\bar{\mathbf{u}}_{\mathrm{s},k-1}$ in the form

$$\mathbf{\Phi} = \left.\frac{\partial}{\partial \mathbf{x}_{\mathrm{obs}}}\mathbf{F}\left(\mathbf{x}_{\mathrm{obs}}, \bar{\mathbf{u}}_{\mathrm{s},k-1}, \mathbf{0}\right)\right|_{\mathbf{x}_{\mathrm{obs}}=\hat{\mathbf{x}}^+_{\mathrm{obs},k-\frac{1}{2}}} \tag{17a}$$

$$\mathbf{G} = \left.\frac{\partial}{\partial \mathbf{w}_k}\mathbf{F}\left(\hat{\mathbf{x}}_{\mathrm{obs},k-\frac{1}{2}}, \bar{\mathbf{u}}_{\mathrm{s},k-1}, \mathbf{w}_k\right)\right|_{\mathbf{w}_k=\mathbf{0}} \tag{17b}$$

$$\hat{\mathbf{x}}^-_{\mathrm{obs},k} = \mathbf{F}\left(\hat{\mathbf{x}}_{\mathrm{obs},k-\frac{1}{2}}, \bar{\mathbf{u}}_{\mathrm{s},k-1}, \mathbf{0}\right) \tag{17c}$$

$$\mathbf{P}^-_k = \mathbf{\Phi}\mathbf{P}^+_{k-\frac{1}{2}}\mathbf{\Phi}^{\mathrm{T}} + \mathbf{G}\mathbf{Q}\mathbf{G}^{\mathrm{T}}, \tag{17d}$$

see, e.g., [22] for the theory and basics of EKF. In (17), $\mathbf{Q}$ and $\mathbf{R}$ denote the positive definite covariance matrices of the process noise $\mathbf{w}$ and the measurement noise $\mathbf{v}$, respectively. $\mathbf{P}_0$ and $\hat{\mathbf{x}}_{\mathrm{obs},0}$ are specified as initial values.

The observer is called at $t = kT_\mathrm{s}$ since the real-time system is aligned with the update of the control input. To approximately compensate for the calculation time of the observer and the controller, it is meaningful to use a prediction to $t = (k+1)\,T_\mathrm{s}$. Thus the observer is calculated following the sequence:

- Update $\hat{\mathbf{x}}^-_{\mathrm{obs},k-\frac{1}{2}}$ to $\hat{\mathbf{x}}^+_{\mathrm{obs},k-\frac{1}{2}}$ using $\tilde{\mathbf{i}}_{\mathrm{s},k}$, using (16)
- Predict $\hat{\mathbf{x}}^+_{\mathrm{obs},k-\frac{1}{2}}$ to $\hat{\mathbf{x}}^-_{\mathrm{obs},k}$ with $\bar{\mathbf{u}}_{\mathrm{s},k-1}$, using (17)
- Predict $\hat{\mathbf{x}}^-_{\mathrm{obs},k}$ to $\hat{\mathbf{x}}^-_{\mathrm{obs},k+\frac{1}{2}}$ with $\bar{\mathbf{u}}_{\mathrm{s},k}$, using (17)
- Predict $\hat{\mathbf{x}}^-_{\mathrm{obs},k+\frac{1}{2}}$ to $\hat{\mathbf{x}}^-_{\mathrm{obs},k+1}$ with $\bar{\mathbf{u}}_{\mathrm{s},k}$, using (17)

It is important to note that the chosen machine parameters cannot be estimated at every operating point. E.g., the rotor resistance is not observable if there are no rotor currents [20]. To take this into account in the observer, the update steps of $\hat{R}_\mathrm{r}$, and the corresponding entries in the covariance matrix $\mathbf{P}_k$, are not executed at low rotor currents.

As stated before, the main innovation of the proposed observer is the exact timing of the observer, as described in (16) and (17). In order to show the improvement of this timing, the observer will be compared to an EKF, which uses the timing typically utilized in the literature. In particular, the exact timing of the current measurement point is not considered in the sequence of the classic EKF:

- Update $\hat{\mathbf{x}}^-_{\mathrm{obs},k}$ to $\hat{\mathbf{x}}^+_{\mathrm{obs},k}$ using $\tilde{\mathbf{i}}_{\mathrm{s},k}$
- Predict $\hat{\mathbf{x}}^+_{\mathrm{obs},k}$ to $\hat{\mathbf{x}}^-_{\mathrm{obs},k+1}$ with $\bar{\mathbf{u}}_{\mathrm{s},k}$

IV. Simulation and Experimental Results

The proposed observer is first investigated by simulations. To do so, the detailed continuous-time model of the induction machine, including the PWM according to (9), is implemented using Matlab/Simulink. The EKF is combined with a classic field-oriented control strategy [25], which allows control of the test machine's torque using the proposed observer's estimated states and parameters. These simulations are performed at three different sampling times (PWM frequencies $f_\mathrm{s} = 10\,\mathrm{kHz}$, $f_\mathrm{s} = 1\,\mathrm{kHz}$, and $f_\mathrm{s} = 500\,\mathrm{Hz}$) at rotational speeds up to 1500 rpm. A single current measurement in the center of the PWM period is used for these simulation studies, see (11).

Remark 1: The speed of 1500 rpm at a PWM frequency $f_\mathrm{s} = 500\,\mathrm{Hz}$ corresponds to a sample-to-fundamental frequency ratio of 20, which is a low value for practical applications, e.g., [11]. It is the same ratio as in an automotive traction drive with an electrical speed of 30 krpm and 10 kHz PWM frequency [3], [4]. It must be noted that the low PWM frequency of $f_\mathrm{s} = 500\,\mathrm{Hz}$ is utilized since the test bench used for the experimental results has a limited speed range of approx. 2000 rpm. Thus, a low PWM frequency is chosen to obtain a low sample-to-fundamental frequency ratio.

Table I shows the main parameters of the used machine. The covariance matrix $\mathbf{R}$ of the measurement noise is adjusted to match the measured noise on the test bench. The entries of the process disturbances' covariance matrix are tuned in simulations, where the entries for R_r and M are chosen to yield a sufficiently slow estimation. The initial values for $\mathbf{P}_0$ and $\hat{\mathbf{x}}_{\mathrm{obs},0}$ are chosen empirically. The selected parameters are listed in Table II. For the assessment of the observer accuracy, the difference between the estimated torque $T(\hat{\mathbf{x}}_{\mathrm{obs}})$ and the simulated torque T is used, i.e., $e_\mathrm{T} = T - T(\hat{\mathbf{x}}_{\mathrm{obs}})$, since it is of primary importance.

TABLE I
MACHINE PARAMETERS.

M	L_σ	R_r	R_s	Z_p
35.0 mH	5.7 mH	254 mΩ	217 mΩ	1

TABLE II
EKF CONFIGURATION

$\mathbf{Q}$	$T_\mathrm{s}^2\,\mathrm{diag}\left(100,\ 100,\ 100,\ 100,\ 1.2\cdot10^{-3},\ 0.64\right)$
$\mathbf{R}$	$1.5\cdot10^{-4}\mathbf{I}$
$\mathbf{P}_0$	$\mathrm{diag}\left(10^{-5},\ 10^{-5},\ 10^{-5},\ 10^{-5},\ 10^{-8},\ 10^{-7}\right)$
$\hat{\mathbf{x}}_{\mathrm{obs},0}$	$\left[0,\ 10^{-3},\ 0,\ 10^{-3},\ 0.035,\ 0.254\right]^{\mathrm{T}}$

Figure 2 shows the simulation results for various rotational speeds and torques. Both the results of the proposed estimator (prop.) and the classic EKF implementation (classic) are depicted. It can be seen that both observers have a very high estimation accuracy for a high sampling rate of 10 kHz. For lower PWM frequencies and thus lower sample-to-fundamental frequency ratios, the advantages of the proposed observer become evident. In particular, for the very low value of $f_\mathrm{s} = 500\,\mathrm{Hz}$, the classical observer yields large deviations, while the proposed method is able to keep a high estimation accuracy.

To show the practical feasibility, the described observer was also evaluated on a test bench, see [26] for more details of the test bench. The observer and the control strategy are implemented on a dSPACE real-time system, and a load machine allows the adjustment of the rotational speed of the setup. One main limitation of test bench measurements is that it is difficult to obtain accurate torque measurements due to inherent friction. Furthermore, the exact machine parameters are unavailable, yielding model deviations from the real motor. Since the main task of the measurements is to evaluate the influence of the sample-to-fundamental frequency ratio on the estimation accuracy, and since it was shown in simulation that for 10 kHz, the proposed and the classical observer

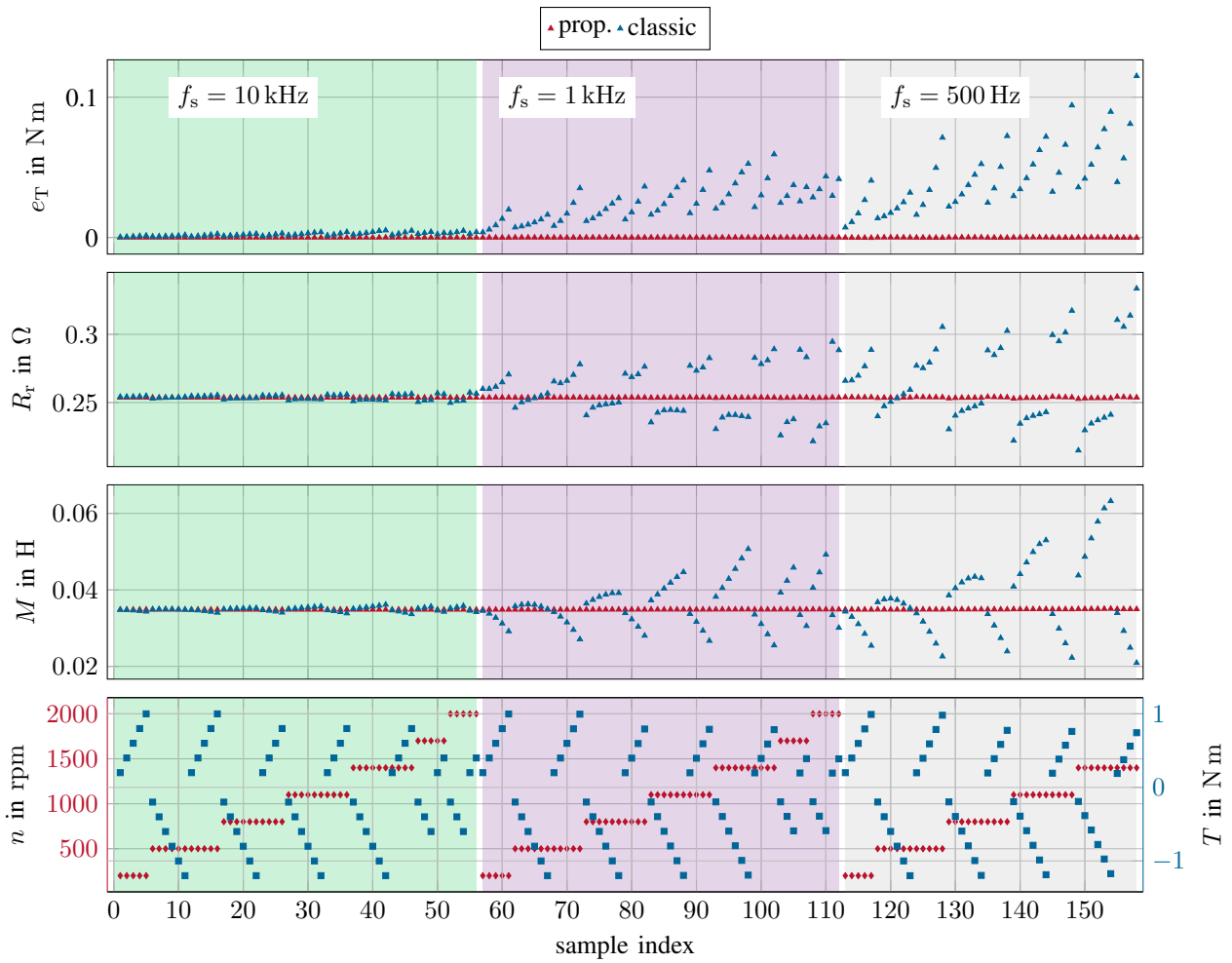

Fig. 2. Simulation results for sample frequencies of $f_s = 500\,\mathrm{Hz}$, $f_s = 1\,\mathrm{kHz}$ and $f_s = 10\,\mathrm{kHz}$.

have similar good results, the results in Figure 3 give the deviation of the measurements at $1\,\mathrm{kHz}$ and $500\,\mathrm{Hz}$ to the results at $10\,\mathrm{kHz}$, i.e., $e_{T,10} = T\left(\hat{\mathbf{x}}_{\mathrm{obs},10\,\mathrm{kHz}}\right) - T\left(\hat{\mathbf{x}}_{\mathrm{obs}}\right)$, $e_{R_\mathrm{r},10} = \hat{R}_{\mathrm{r},10\,\mathrm{kHz}} - \hat{R}_\mathrm{r}$ and $e_{M,10} = \hat{M}_{10\,\mathrm{kHz}} - \hat{M}$.

The results in Fig. 3 show that the proposed observer strategy gives significantly better results than the classical observer, although the overall errors increase compared to the simulation results. This can be partially attributed to the fact that the errors also include the control error since achieving high control accuracy at a low sample-to-fundamental frequency ratio is difficult. To show that this effect is also relevant in the simulation results when referring the results at $1\,\mathrm{kHz}$ and $500\,\mathrm{Hz}$ to the results at $10\,\mathrm{kHz}$, Fig. 3 also shows the corresponding simulation results. The simulation and measurement results are in good agreement. Thus, it can be concluded that the estimation accuracy for the torque in the measurements is similar to the simulation results.

Another important issue is the accuracy and feasibility of the estimated parameters. It can be seen that while the proposed observer yields physically meaningful parameters in all scenarios, the classical approach partially gives unreasonable results, in particular for M. It is important to note that it is, of course, expected that M can vary due to magnetic saturation. The large deviations of the classical observer in the experiments can not be physically explained. While this may be fine for the torque accuracy in a given application, it may still affect the performance of a controller or trajectory planning algorithm that uses incorrectly estimated parameters.

V. Conclusions

This work investigated the practical timing aspects of implementing an observer for induction machines, particularly for low sample-to-fundamental frequency ratios. It was shown that since the current measurement is typically performed in the center of a PWM, the corrector step of state-space observers must be performed considering the state at this time. Furthermore, it was demonstrated how to consider the timing of the predictor steps correctly. The simulation and experimental results proved that the proposed observer strategy significantly improves the estimation

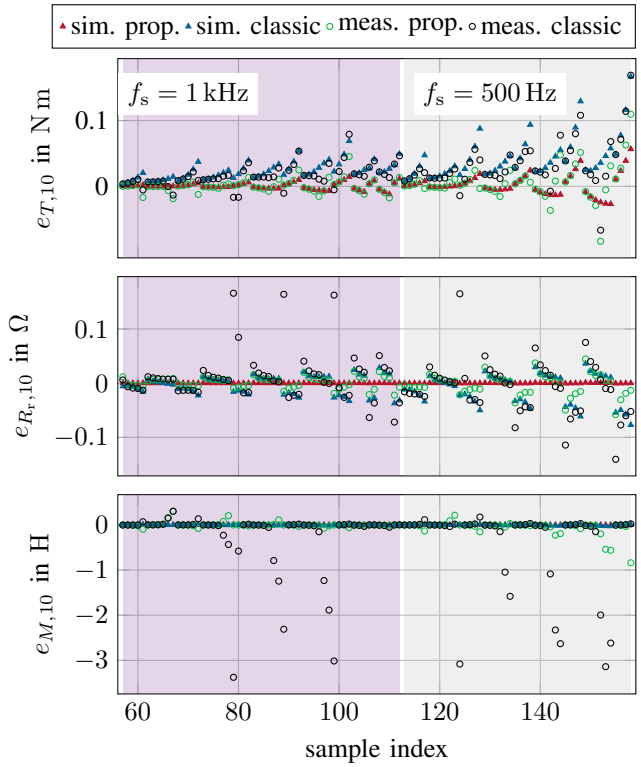

Fig. 3. Measurements with sample frequencies of $f_s = 500\,\mathrm{Hz}$ and $f_s = 1\,\mathrm{kHz}$.

accuracy compared to a classical approach that does not account for this effect. The correct consideration of the timing of the measurements within the observer design will have an increasing relevance due to the trend for motor construction with very high rotational speed with limited PWM frequencies of the inverter.

References

[1] C. Liu, K. T. Chau, C. H. T. Lee, and Z. Song, "A Critical Review of Advanced Electric Machines and Control Strategies for Electric Vehicles," *Proceedings of the IEEE*, vol. 109, no. 6, pp. 1004–1028, jun 2021.

[2] H. A. Toliyat, E. Levi, and M. Raina, "A review of RFO induction motor parameter estimation techniques," *IEEE Transactions on Energy Conversion*, vol. 18, no. 2, pp. 271–283, jun 2003.

[3] L. Shao, A. E. H. Karci, D. Tavernini, A. Sorniotti, and M. Cheng, "Design Approaches and Control Strategies for Energy-Efficient Electric Machines for Electric Vehicles - A Review," *IEEE Access*, vol. 8, pp. 116 900–116 913, 2020.

[4] J. Reimers, L. Dorn-Gomba, C. Mak, and A. Emadi, "Automotive Traction Inverters: Current Status and Future Trends," *IEEE Transactions on Vehicular Technology*, vol. 68, no. 4, pp. 3337–3350, apr 2019.

[5] A. E. Gaspar, Y. Xu, and R. D. Lorenz, "A simpler gopinath-style flux observer without a constant speed assumption for low and high sampling-to-fundamental frequency ratios for induction machines," in *IEEE Energy Conversion Congress and Exposition, ECCE*, Baltimore, MD, USA, 2019, pp. 1832–1839.

[6] P. L. Jansen and R. D. Lorenz, "A Physically Insightful Approach to the Design and Accuracy Assessment of Flux Observers for Field Oriented Induction Machine Drives," *IEEE Transactions on Industry Applications*, vol. 30, no. 1, pp. 101–110, 1993.

[7] R. D. Lorenz and D. W. Novotny, "Observer-Based Direct Field Orientation: Analysis and Comparison of Alternative Methods," *IEEE Transactions on Industry Applications*, vol. 30, no. 4, pp. 945–953, 1994.

[8] N. T. West and R. D. Lorenz, "Digital implementation of stator and rotor flux-linkage observers and a stator-current observer for deadbeat direct torque control of induction machines," *IEEE Transactions on Industry Applications*, vol. 45, no. 2, pp. 729–736, 2009.

[9] H. Kim, M. W. Degner, J. M. Guerrero, F. Briz, and R. D. Lorenz, "Discrete-time current regulator design for AC machine drives," *IEEE Transactions on Industry Applications*, vol. 46, no. 4, pp. 1425–1435, jul 2010.

[10] Y. Wang, S. Tobayashi, and R. D. Lorenz, "A Low-Switching-Frequency Flux Observer and Torque Model of Deadbeat-Direct Torque and Flux Control on Induction Machine Drives," *IEEE Transactions on Industry Applications*, vol. 51, no. 3, pp. 2255–2267, may 2015.

[11] Y. Xu, C. Morito, and R. D. Lorenz, "Accurate Discrete-Time Modeling for Improved Torque Control Accuracy for Induction Machine Drives at Very Low Sampling-to-Fundamental Frequency Ratios," in *IEEE Transportation Electrification Conference and Expo, ITEC*, Novi, Michigan, USA, 2019.

[12] O. Stoicuçã and T. C. Pana, "Design and stability study of an induction motor vector control system with extended rotor-flux and rotor-resistance gopinath observer," in *8th International Symposium on Advanced Electromechanical Motion Systems and Electric Drives Joint Symposium, ELECTROMOTION*, Lillie, France, 2009, pp. 1–8.

[13] H. Kubota, K. Matsuse, and T. Nakano, "DSP-Based Speed Adaptive Flux Observer of Induction Motor," *IEEE Transactions on Industry Applications*, vol. 29, no. 2, pp. 344–348, 1993.

[14] E. Zerdali, "A Comparative Study on Adaptive EKF Observers for State and Parameter Estimation of Induction Motor," *IEEE Transactions on Energy Conversion*, vol. 35, no. 3, pp. 1443–1452, 2020.

[15] S. Dutta, A. Yoo, Y. Shi, and V. C. Peddi, "A Comparison of Induction Machine Rotor Flux Observers in Stationary Reference Frame for Rotor Flux Position Estimation," in *IEEE Energy Conversion Congress and Exposition, ECCE*, Detroit, MI, USA, 2022, pp. 1–8.

[16] T. Kataoka, S. Toda, and Y. Sato, "On-line estimation of induction motor parameters by extended Kalman filter," in *Fifth European Conference on Power Electronics and Applications*, Brighton, UK, 1993, pp. 325–329.

[17] H. Gashtil, V. Pickert, D. John Atkinson, D. Giaouris, and M. Dahidah, "On-line estimation of magnetizing inductance and rotor resistance in extended kalman-filter for induction machines," in *2nd European Conference on Electrical Engineering and Computer Science, EECS*, Bern, Switzerland, 2018, pp. 582–588.

[18] L. C. Zai, C. L. DeMarco, and T. A. Lipo, "An Extended Kalman Filter Approach to Rotor Time Constant Measurement in PWM Induction Motor Drives," *IEEE Transactions on Industry Applications*, vol. 28, no. 1, pp. 96–104, 1992.

[19] S. Yang, D. Ding, X. Li, Z. Xie, X. Zhang, and L. Chang, "A Decoupling Estimation Scheme for Rotor Resistance and Mutual Inductance in Indirect Vector Controlled Induction Motor Drives," *IEEE Transactions on Energy Conversion*, vol. 34, no. 2, pp. 1033–1042, jun 2019.

[20] R. Marino, P. Tomei, and C. M. Verrelli, *Induction Motor Control Design*, ser. Advances in Industrial Control. London: Springer London, 2010.

[21] J. Ma, X. Wang, F. Blaabjerg, L. Harnefors, and W. Song, "Accuracy Analysis of the Zero-Order Hold Model for Digital Pulse Width Modulation," *IEEE Transactions on Power Electronics*, vol. 33, no. 12, pp. 10 826–10 834, dec 2018.

[22] D. Simon, *Optimal State Estimation*. Hoboken, NJ, USA: John Wiley & Sons, Inc., 2006.

[23] N. P. Quang and J.-A. Dittrich, *Vector Control of Three-Phase AC Machines*, ser. Power Systems. Berlin, Heidelberg: Springer Berlin Heidelberg, 2015.

[24] B. Weber, T. Brandt, and A. Mertens, "Compensation of switching dead-time effects in voltage-fed PWM inverters using FPGA-based current oversampling," in *IEEE Applied Power Electronics Conference and Exposition, APEC*, Long Beach, CA, USA, 2016, pp. 3172–3179.

[25] R. W. De Doncker, D. W. Pulle, and A. Veltman, *Advanced Electrical Drives*, ser. Power Systems. Cham: Springer International Publishing, 2020.

[26] G. Janisch, A. Kugi, and W. Kemmetmüller, "Model calibration strategy for energy-efficient operation of induction machines," *IFAC-PapersOnLine*, vol. 55, no. 20, pp. 307–312, jan 2022.